ACS APPLIED MATERIALS & INTERFACES

Research Article

www.acsami.org

Fabrication of Artificially Stacked Ultrathin ZnS/MgF_2 Multilayer Dielectric Optical Filters

Garima Kedawat,*[,†] Subodh Srivastava,[†] Vipin Kumar Jain,[‡] Pawan Kumar,[§] Vanjula Kataria,[§] Yogyata Agrawal,[§] Bipin Kumar Gupta,*[,§] and Yogesh K. Vijay[†]

[†]Department of Physics, University of Rajasthan, Jaipur 302055, India

[‡]Department of Physics, Institute of Engineering and Technology, JK Lakshmipat University, Jaipur, India

[§]CSIR - National Physical Laboratory, Dr. K S Krishnan Road, New Delhi, India

Supporting Information

ABSTRACT: We report a design and fabrication strategy for creating an artificially stacked multilayered optical filters using a thermal evaporation technique. We have selectively chosen a zinc sulphide (ZnS) lattice for the high refractive index (n = 2.35) layer and a magnesium fluoride (MgF_2) lattice as the low refractive index (n = 1.38) layer. Furthermore, the microstructures of the ZnS/MgF_2 multilayer films are also investigated through TEM and HRTEM imaging. The fabricated filters consist of high and low refractive 7 and 13 alternating layers, which exhibit a reflectance of 89.60% and 99%, respectively. The optical microcavity achieved an average transmittance of 85.13% within the visible range. The obtained results suggest that these filters could be an exceptional choice for next-generation antireflection coatings, high-reflection mirrors, and polarized interference filters.

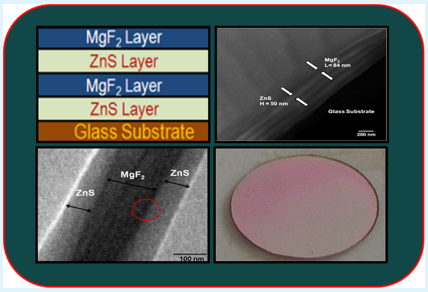

KEYWORDS: *zinc sulphide, magnesium fluoride, multilayer thin film, X-ray diffraction, UV−vis spectroscopy*

INTRODUCTION

Recently, the interference phenomenon is being used in ultrathin filters for their extensive applications in optics to control electromagnetic waves. Such types of filters are designed with quarter wave (QW) stacks of alternating high and low refractive index ultrathin layers deposited on a substrate, making thin multilayered structures having the property of reflecting some wavelengths and transmitting the others.[1] Such a filter can be tailored according to high reflectance or transmission toward a desired wavelength or a range of wavelengths by altering the design of the thin film components, as in the refractive index and optical thickness of layers. Therefore, the tuning of these filters provides broad availability with narrow and wide wavelength windows of transmission/reflection and are usually defined through their central wavelength, full width half-maximum (fwhm), peak transmittance T_0, and rejection band.[2] These filters are fascinating in a wide field of applications, such as antireflection coatings, high-reflection mirrors, and polarized interference filters.[3−12] Filters in the visible region are generally used to increase the efficiency of optical systems by reducing the reflections that occur at each lens' surface. They can also be used as reflective filters for sunglasses or smart fashion eyewear. Narrow band filters from the UV through the visible range are used in sensing applications to pass wavelengths of interest to a detector. The typical interference filters are composed of several spacer regions surrounded by multilayer reflectors.[13] The reflector region consists of alternate layers of materials of high and low refractive indices. The optical thickness of each of the layers of the reflector region is one-quarter of the central wavelength so that beams reflected by each layer undergo destructive interference for selective wavelengths. The optical thickness of the spacers, also known as cavities, is half the central wavelength. The optical interference between the layers gives rise to the band-pass-filter functionality.[14]

We carried out research in the interference phenomenon of the extraordinary ZnS/MgF_2 ultrathin multilayer optical filter. ZnS has a direct and wide band gap of 3.5−3.8 eV, a high refractive index of 2.35 at 550 nm[15] with low optical absorption in the visible and infrared spectral regions, and transmission of high energy photons,[16−19] whereas MgF_2 has a low refractive index of 1.38 at 550 nm[15] and a wide transmittance range. The extensive studies on the optical properties of ZnS and MgF_2 films[20−22] report them to be quite useful for optical coatings.[23−28] The high value of refractive index contrast between the two material types (n_H/n_L) is most desirable in the design of the multilayered structure as it keeps the number of layers and their physical thickness to a minimum for a given spectral function. The refractive index of MgF_2 is close to the square root of the refractive index of ZnS. For these reasons, ZnS and MgF_2 are suitable choices for the production of interference optical filters. Hence, using just a few layers, surfaces can be obtained with a reflectivity as high as that of a silver mirror (96.6%), and surfaces reflecting more than 99% of

Received: February 19, 2013
Accepted: May 14, 2013
Published: May 14, 2013

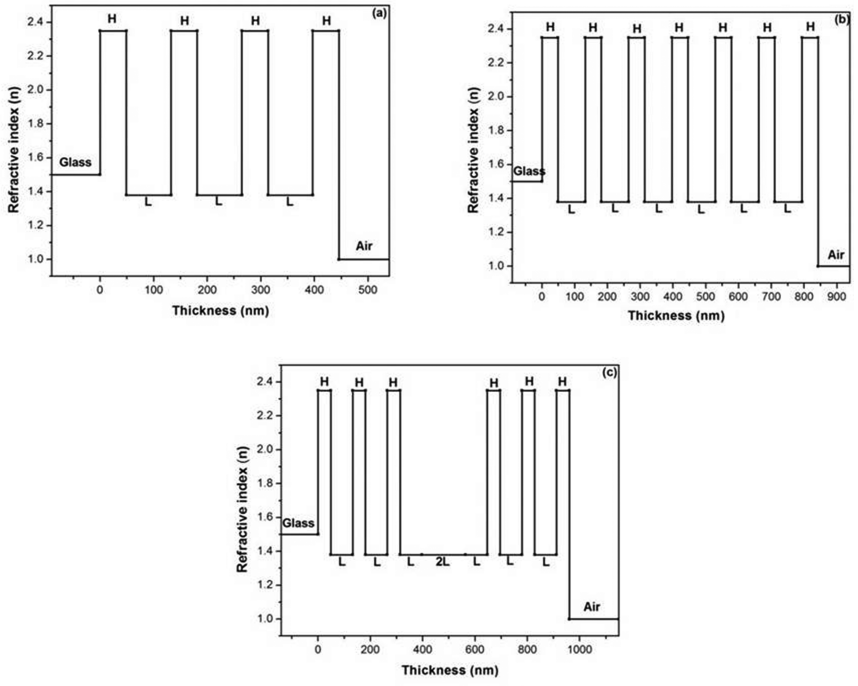

Figure 1. Refractive index profile for (a) Glass/(HL)^{m}H/Air, m = 3, 7 layers, (b) m = 6, 13 layers, and (c) G (HL)^3 2L (LH)^3 A, with quarter wave stacks of alternating high and low indices.

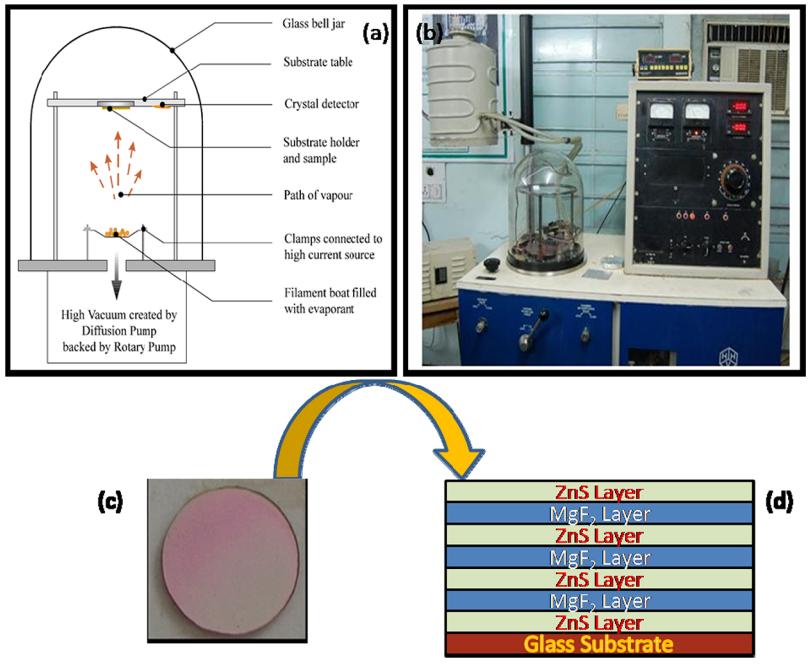

Figure 2. (a, b) Schematic diagram of the system, (c) grown multilayer, and (d) layers of film.

the incident light can be produced with an increase in the number of films. Optimization of the film density and its uniformity over a substrate is an important parameter to be considered well while choosing the fabrication technique for filters.[29−36] Over the years, there have been sustained efforts to improve the quality and reliability of the multilayer optical coatings prepared by physical vapor deposition processes.

EXPERIMENTAL SECTION

In this paper, we describe the designs and process to fabricate the multilayered coating interference filters to improve the optical transmissivity or reflectivity at a chosen wavelength in the visible region. Our design of coating stacks for high reflection and a narrow band-pass filter is illustrated in Figure 1, showing the refractive index profile. In Figure 1a,b, multilayered dielectric stacks exhibit high reflectivity due to constructive interference between light rays reflected from layers with alternating high and low refractive indices that are each one QW thick, that is, Glass (G)/(HL)^{m}H/Air (A), m = 3 and 6, indicating the number of periods in a stack. The designed structures are 7 and 13 layers stacked interference systems. This device is also known as a distributed Bragg reflector (DBR) and exhibit high reflectivity over a wide range (stop band) when the alternating layers have a large index contrast. Figure 1c exhibits the two DBRs separated

dx.doi.org/10.1021/am400612q | ACS Appl. Mater. Interfaces 2013, 5, 4872−4877

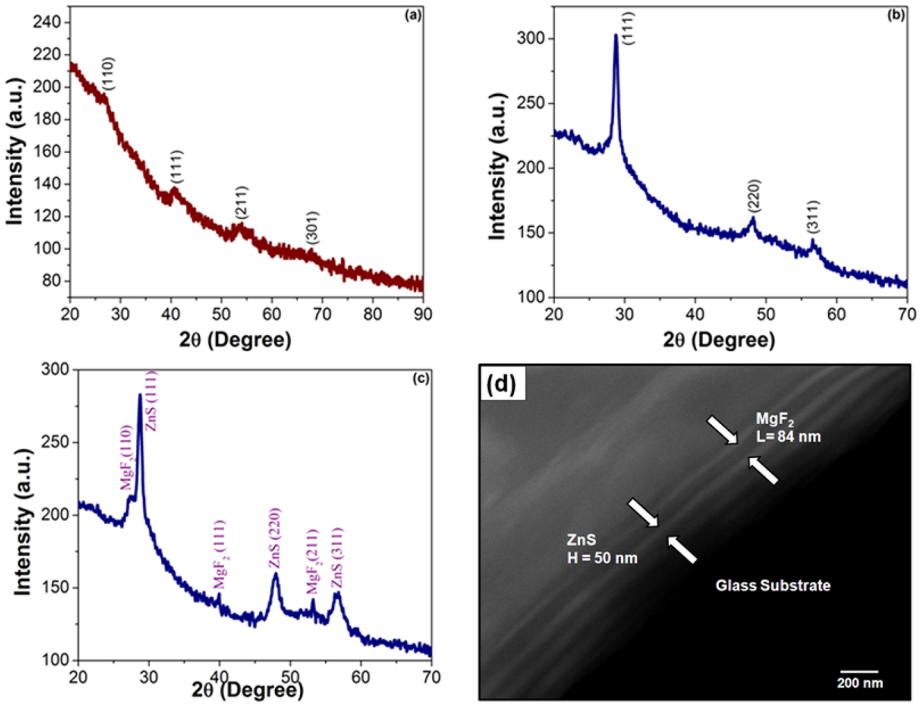

Figure 3. XRD patterns of (a) single layer MgF_2, (b) single layer ZnS, and (c) 13 multilayer ZnS/MgF_2. (d) Cross-sectional SEM image of 7 multilayer ZnS/MgF_2.

by a spacer with a thickness of an integral number of half wavelengths often referred to as the "defect" layer, that is, Glass (G)/$(HL)^3$ 2L $(LH)^3$/Air (A); then, the whole device exhibits a narrow region of high transmission (low reflectivity) within the stop band. This narrow-band filter is also known as a Fabry–Perot cavity or an optical microcavity when the separation is only a few half wavelengths, where H and L represent the QW layers of ZnS and MgF_2 materials, respectively, with a center wavelength of λ_0 = 460 nm.

We fabricated 100 nm single and QW multilayered ultrathin layers of ZnS and MgF_2 for a center wavelength of λ_0 = 460 nm, that is, 50 nm for ZnS and 84 nm for MgF_2 grown on clean glass substrates, which is further evidenced by cross-sectional scanning electron microscopy (SEM), using a thermal evaporation system (HINDHI vacuum coating). The schematic diagrams of the evaporation chamber with descriptions as well as the real system are shown in Figure 2a,b. The system had two position sources, which enabled us to deposit different materials alternatingly in a single vacuum cycle with 5 min long breaks separating each ZnS layer from that of the MgF_2 layers and vice versa. The optical micrograph of a fabricated multilayer and a schematic structure for m = 3 are depicted in Figure 2c,d. During the deposition process, the substrates were kept at ambient temperature and the thickness as well as the deposition rate was controlled and maintained with the help of a quartz crystal monitor. The deposition rates were determined to be 1–2 Å/s for ZnS and 3–4 Å/s for MgF_2 by controlling the current through the evaporation boat. The system was operated at a pressure of about 10^{-5} Torr during deposition.

RESULTS AND DISCUSSION

The gross structural analysis and phase purity of the single layer of MgF_2 and ZnS as well as multilayer were determined by X-ray powder diffraction (XRD) using X′ Pert PRO PANalytical instruments as shown in Figure 3. The prior to the XRD measurements, the calibration of the diffractometer was done with the Si powder (d_{111} = 3.1353 Å). Panels a–c in Figure 3 show the XRD patterns of a single layer of MgF_2, a single layer of ZnS, and 13 multilayers of ZnS/MgF_2, respectively. Figure 3a represents the tetragonal phase of MgF_2 with estimated lattice constants a = 4.611 ± 0.006 Å, b = 4.613 ± 0.011 Å, c = 3.022 ± 0.017 Å, comparable to standard lattice parameters a = 4.625 Å, b = 4.625 Å, c = 3.052 Å (JCPDS, File No. 721150). No impurity peaks were found in the XRD pattern. Similarly, Figure 3b represents the cubic phase of ZnS layer with estimated lattice constants $a = b = c$ = 5.331 ± 0.019 Å as compares to the standard lattice parameters $a = b = c$ = 5.345 Å (JCPDS, File No. 800020) of ZnS.[37,38] The XRD pattern of the ZnS/MgF_2 multilayer is shown in Figure 3c, which exhibits the presence of both pristine phases of MgF_2 and ZnS, respectively. Any additional peaks as well as secondary phases were not observed in the combined phases of the ZnS/MgF_2 composite except pristine ZnS and MgF_2 peaks, which confirms that the lattice diffusion does not occur during the fabrication of alternate layers in the composite system. Moreover, the XRD pattern of MgF_2 appears less crystalline as compared to ZnS, which is further evidenced by high-resolution TEM (HRTEM) images. The estimated particle sizes of a single layer of MgF_2 and ZnS are ∼10 and ∼15 nm, respectively, which are calculated by Scherrer's standard formula. To examine the particle size of the ZnS/MgF_2 composite system, we calculated the particle size of the composite from the XRD pattern of Figure 3c. The estimated particle size is ∼18 nm with respect to the highest peak intensity observed for the composite system. Crystallinity of the as-deposited films appears to depend on the layer thickness. For instance, single layers of ZnS and MgF_2 exhibit only slight crystallinity, whereas the crystallinity improved with an increase of ZnS and MgF_2 multilayers.

Figure 3d shows a cross-sectional backscatter scanning electron microscopic (BSD SEM) image of 7 alternate multilayers of ZnS and MgF_2, respectively, using a Carl Zeiss EVO MA-10 equipment facility. The dark band represents the typical SEM image of the MgF_2 layer and the bright band exhibits the ZnS layer, as shown in Figure 3d, with a thickness of ∼50 ± 2 nm for the ZnS layer and ∼84 ± 2 nm for the MgF_2 layer, respectively. We have also investigated the cross-sectional

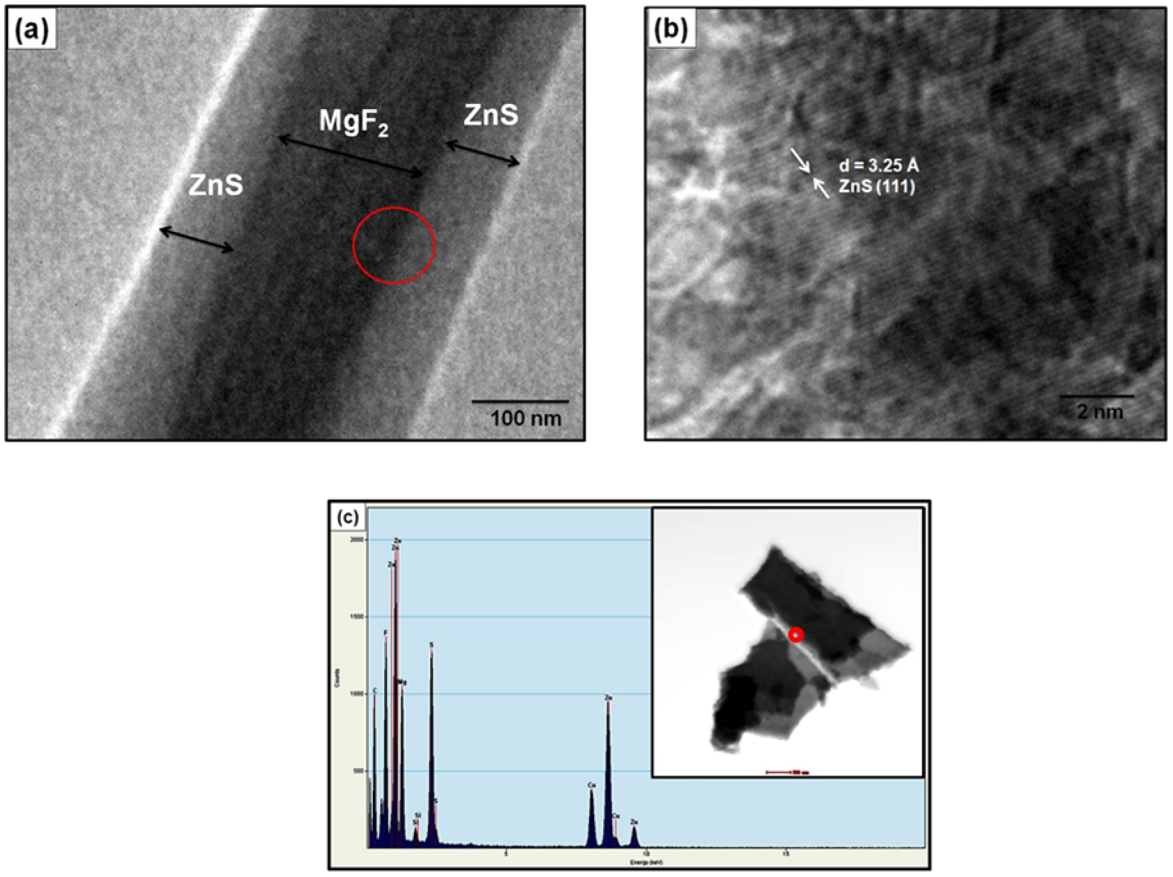

Figure 4. TEM image of (a) artificially stacked pattern (cross-sectional view) of ZnS/MgF_2 multilayer. The marked red circle represents the interface between ZnS and MgF_2. (b) Typical HRTEM image of ZnS/MgF_2 multilayer that clearly demonstrates the interface. (c) The EDAX spectrum of the ZnS/MgF_2 multilayer, inset in (c) shows the TEM image of ZnS/MgF_2 multilayer, the marked by red circle exhibits the place where EDAX spectrum has been taken.

morphology for another multilayer composite through the BSD SEM technique (Figure S1; see details in the Supporting Information). To examine the detailed microstructure information, we performed high-resolution transmission electron microscopy and selected area electron diffraction on artificially stacked multilayer films. We performed transmission electron microscopy (TEM) using a model JEOL-2000FX operated at voltages of 200 kV. Figure 4a clearly shows the cross-sectional TEM image of the film having alternating layers of ZnS and MgF_2 around the design wavelengths of 460 nm. The black band represents MgF_2 and the bright band represents ZnS correspondingly, as shown in Figure 4a. The estimated thicknesses of the ZnS and MgF_2 individually in the artificially stack composite film for the filter are ∼50 and ∼80 nm, respectively. It clearly shows that the thicknesses of designed and deposited films are quite consistent. The interfaces between the ZnS and MgF_2 layers are well-defined; the homogeneous ZnS/MgF_2 alternating structure can be seen in Figure 4a. The typical HRTEM image of ZnS/MgF_2 is shown in Figure 4b. The precise observation image indicates that the ZnS exhibits lattice fringes with an interspacing of 3.25 Å that corresponds to the (111) plane of ZnS, which is further supported by the observed selected area in the electron diffraction pattern (SAED) (Figure S2; see the Supporting Information). Furthermore, the spot EDAX measurement was performed with a reduced beam size and accelerating potential to enhance the signal-to-noise ratio. The qualitative analysis of artificially stacked ZnS/MgF_2 was done using energy-dispersive X-ray analysis, as shown in Figure 4c, which indicates the presence of the Mg, F, Zn, and S elements in the multilayer structure, and Si, C, and O were present due to the carbon-coated grid. We have also demonstrated the cross-sectional EDAX profile spectrum for elements in ZnS/MgF_2 (Figure S3; see details in the Supporting Information).

Figure 5 exhibits the UV−vis spectra (Hitachi-330 Spectrophotometer) of the transmission spectrum of a single MgF_2 layer, a single ZnS layer, and the multilayer ZnS/MgF_2 composite, G $(HL)^m$H A, m = 3,6 DBR and microcavity at a normal incidence angle, respectively. The transmission spectrum of the MgF_2 (100 nm) layer is as shown in Figure 5a. This spectrum consists of an absorption edge between 300 and 370 nm and a transmission plateau from 370 to 800 nm. The maximum transmittance of 85−90% extends from 400 to 700 nm. The transmission spectrum of a thin (100 nm) ZnS layer is shown in Figure 5b, which clearly demonstrates the exceptional optical quality in relation to the low absorption characteristic and film homogeneity over the visible spectral region. Such optical properties of the thin layer are necessary to provide high transmission and also color balance over the visible spectrum. The high contrast of the interference fringes seen in the transmission spectra indicates the high optical quality of the thin-film surfaces. Figure 5c shows the transmittance spectra for DBR filters prepared by alternate 7 and 13 layers of ZnS and MgF_2, respectively, at a normal incidence angle for the visible range. These spectra clearly show that optical multilayer filters have been obtained in accordance

dx.doi.org/10.1021/am400612q | ACS Appl. Mater. Interfaces 2013, 5, 4872−4877

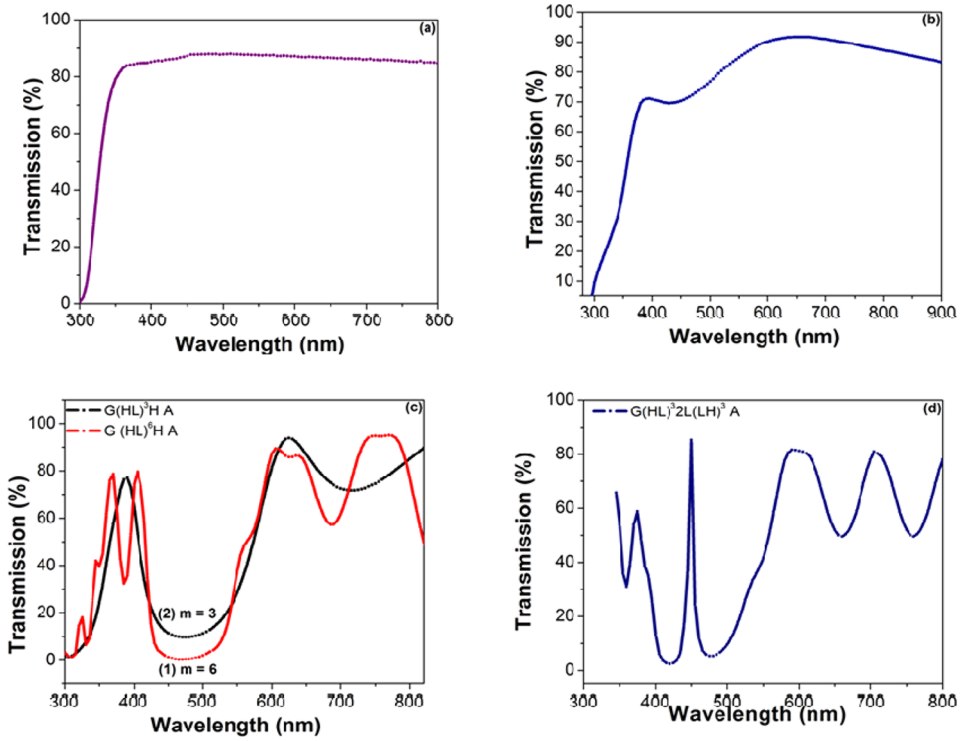

Figure 5. Transmission spectra of (a) MgF_2 layer, (b) ZnS layer, (c) G $(HL)^m$H A, m = 3,6, distributed Bragg reflector, and (d) G $(HL)^3$ 2L $(LH)^3$ A, microcavity at normal incidence angle.

with the design G $(HL)^m$H A, with m = 3 and 6. In Figure 5c, curve (1), corresponding to m = 3, shows the transmittance of 9.3%, whereas curve (2), corresponding to m = 6, shows the transmittance of 0.5% at 470 nm; that is, high and low refractive 7 and 13 alternate layers exhibit a reflectance of 89.60% and 99%, respectively. These spectra clearly revealed that the transmittance decreases and reflectance increases around the reference wavelength of 470 nm when the number of HL pairs increases; that is, the minimum transmittance or maximum reflectance has been observed, which served as a reflectance filter. It has also been observed that the visible reflectance approaches 100% due to addition of HL pairs. The higher reflectance value can be achieved by designing a high−low index quarter wave "HL" film pairs; that is, such alternate low and high index quarter wave films raise the reflectance to a very high value at the reference wavelength position. The number of layers are 7 and 13 and the total thickness of the composite are 452 and 854 nm, corresponding to m = 3 and 6, respectively. The stop band of the 3- and 6-bilayer DBR is centered at 470 nm, having a full width at half-maximum (fwhm) of 170 and 143 nm, respectively. It was observed that the layer matching technique is very useful in controlling the shape and improving the transmittance or reflectance through the filter by increasing the HL pairs. In the alternate filter design approach, the experimental transmission spectrum of the microcavity is shown in Figure 5d at the normal incidence. These figures clearly show that the optical multilayer filters have been obtained in accordance with the design G $(HL)^3$ 2L $(LH)^3$ A. The transmittance spectrum shows a sharp characteristic peak with a maximum (85.13%) at the reference wavelength of 460 nm. The width (fwhm) of the transmittance spectra is observed at 9 nm. There are small deviations at the peak position, which may be attributed to the shift of the center wavelength λ_0 during the coating procedure. Thus, it can be easily demonstrated that the average reflectance of the multilayer filter can be tuned as desired with the introduction of the cavities in the filter.

CONCLUSION

We describe two different designs for the fabrication of multilayered interference filters with different transmission or reflection characteristics. A vacuum thermal deposition technique was used at room temperature to realize these interference filters composed of multilayered artificial stacks of dielectric ultrathin layers of zinc sulphide (ZnS) and magnesium fluoride (MgF_2) with selective thicknesses and refractive indices. The XRD analysis reveals that these fabricated multilayer ultrathin alternating layers correspond to the specific structures of ZnS and MgF_2 materials. The microstructure studies of artificially stacked multilayers have been successfully demonstrated through TEM and HRTEM. The experimental transmittance spectra have good agreement with the spectra calculated based on the optical multilayer film theory. The reflected bands for 7 and 13 layer filters have a full width at a half-maximum (fwhm) of about 170 and 143 nm, respectively. Moreover, in a multilayer structure, the variation of reflectivity with wavelength becomes more pronounced with increasing the number of HL pairs. Apart from the above conclusions on the primary filter, we also observed that, within the visible range, a high transmittance of 85.13% was offered by secondary filters, and hence, we concluded that, due to the cavity effect, transmittance (reflectance ∼ 15%) can be easily tailored at the center wavelength. Furthermore, it has been inferred that the primary filter having 7 and 13 alternating layers of ZnS and MgF_2 achieved an average reflectance of 89.60% and 99%, respectively, at a wavelength of 470 nm within the visible spectrum, which is useful in next-generation

laser technologies, advanced photometric measurements, and high-resolution mirror coatings.

■ ASSOCIATED CONTENT

Supporting Information

Cross-sectional SEM, SAED, and EDAX line-spectrum of ZnS/MgF_2 multilayer is discussed and described in the Supporting Information. This material is available free of charge via the Internet at http://pubs.acs.org.

■ AUTHOR INFORMATION

Corresponding Author

*E-mail: kedawat08@gmail.com (G.K.), bipinbhu@yahoo.com (B.K.G.).

Notes

The authors declare no competing financial interest.

■ ACKNOWLEDGMENTS

The authors gratefully acknowledge the University Grant Commission (UGC), Government of India, for financial assistance and the Department of Physics, University of Rajasthan, Jaipur (India), for experimental facilities to carry out this work.

■ ABBREVIATIONS

ZnS, zinc sulphide
MgF_2, magnesium fluoride
QW, quarter wave
DBR, distributed Bragg reflector

■ REFERENCES

(1) Habubi, N. F.; Mishjil, K. A.; Rashid, H. G.; Mansour, H. L. *Mod. Phys. Lett. B* **2010**, *24*, 2821−2829.
(2) Thelen, A. *Design of Optical Interference Coating*; McGraw Hill: New York, 1989; pp 115−120.
(3) Lee, C. C.; Chen, S. H.; Kuo, C. C.; Wei, C. Y. *Opt. Express* **2007**, *15*, 15228−15233.
(4) Willey, R. R. *Thin Solid Films* **2001**, *1*, 398−399.
(5) Finkelstein, N. D.; Lempert, W. R.; Miles, R. B. *Opt. Lett.* **1997**, *22*, 537−539.
(6) Piegari, A.; Bulir, J. *Appl. Opt.* **2006**, *45*, 3768−3773.
(7) Piegari, A.; Bulir, J.; Krasilnikova Sytchkova, A. *Appl. Opt.* **2008**, *47*, C151−C156.
(8) Tan, M. Q.; Lin, Y. C.; Zhao, D. Z. *Appl. Opt.* **1997**, *36*, 827−830.
(9) Zheng, S. Y.; Lit, W. Y. *Can. J. Phys.* **1983**, *61*, 361−368.
(10) Augustsson, T. *IEEE Photonics Technol. Lett.* **2001**, *13*, 215−217.
(11) Postava, K.; Pistora, J.; Kojima, M.; Kikuchi, K.; Endo, K.; Yamaguchi, T. *Opt. Express* **2003**, *11*, 610−616.
(12) Lee, C. C.; Wu, K. *Opt. Lett.* **2007**, *32*, 2118−2120.
(13) Macleod, H. A. *Thin Film Optical Filters*, 4th ed.; Optics and Optoelectronics Series; Institute of Physics Publishing: Bristol, England, 2003; pp 5−9.
(14) Fischer, R. E.; Gale, B. T. *Optical System Design*; McGraw-Hill: New York, 2000; pp 423−430.
(15) Palik, E. D. *Handbook of Optical Constants of Solids*; Academic Press: San Diego, CA, 1998; Vol. 3, pp 998−1000.
(16) Menner, R.; Dimmler, B.; Mauch, R. H.; Schock, H. W. *J. Cryst. Growth* **1988**, *86*, 906−913.
(17) Nomura, R.; Murai, T.; Toyosaki, T.; Matsuda, H. *Thin Solid Films* **1995**, *271*, 4−7.
(18) Yoo, Y. Z.; Chikyow, T.; Ahmet, P.; Jin, Z. W.; Kawasaki, M.; Koinuma, H. *J. Cryst. Growth* **2002**, *237*, 1594−1598.
(19) Venkata Subbaiah, Y. P.; Prathap, P.; Ramakrishna Reddy, K. T. *Appl. Surf. Sci.* **2006**, *253*, 2409−2415.
(20) Perales, F.; Herrero, J. M.; Jaque, D.; de las Heras, C. *Opt. Mater.* **2007**, *29*, 783−787.
(21) Nadeem, M. Y.; Ahmed, W. *Turk. J. Phys.* **2000**, *24*, 651−659.
(22) Siqueiros, J. M.; Machorro, R.; Regalado, L. E. *Appl. Opt.* **1988**, *27*, 2549−2553.
(23) Protopapa, M. L.; De Thomasi, F.; Perrone, M. R.; Piegari, A.; Masetti, E.; Ristau, D.; Quesnel, E.; Duparre, A. *J. Vac. Sci. Technol., A* **2001**, *19*, 681−688.
(24) Ristau, D.; Ganster, S.; Bosch, S.; Duparr, A.; Masetti, E.; Borrull, J.; Kiriakidis, G.; Peirc, F.; Quesnel, E.; Tikhonravov, A. *Appl. Opt.* **2002**, *41*, 3196−3204.
(25) Nadeem, M. Y.; Ahmed, W.; Wasiq, M. F. *J. Res. (Sci.)* **2005**, *16*, 105−112.
(26) Dedova, T.; Krunks, M.; Volobujeva, O.; Oja, I. *Phys. Status Solidi C* **2005**, *2*, 1161−1166.
(27) Perales, F.; de las Heras, C.; Agullo-Rueda, F. *J. Phys. D: Appl. Phys.* **2008**, *41*, 225405−225410.
(28) Palik, E. D. *Handbook of Optical Constants of Solids*; Academic Press: Boston, MA, 1985; Vol. *I*, pp 597−599.
(29) McNally, J. J.; Jungling, K. C.; Williams, F. L.; McNeil, J. R. *J. Vac. Sci. Technol., A* **1987**, *5*, 2145−2149.
(30) Pongratz, S.; Zoller, A. *J. Vac. Sci. Technol., A* **1992**, *10*, 1897−1904.
(31) Jaing, C. C.; Chen, H. C.; Lee, C. C. *Opt. Rev.* **2009**, *16*, 396−399.
(32) Matthews, A. *J. Vac. Sci. Technol., A* **2003**, *21*, 224−231.
(33) Jin, Y.; Shimada, M.; Ono, T. *J. Vac. Sci. Technol., A* **2004**, *22*, 2431−2436.
(34) Bauer, S.; Klippe, L.; Rothhaar, U.; Kuhr, M. *Thin Solid Films* **2003**, *442*, 189−193.
(35) Keddie, J. L.; Giannelis, E. P. *Mater. Res. Soc. Symp. Proc.* **1998**, *1800*, 387−392.
(36) Partlow, D. P.; O'Keefe, T. W. *Appl. Opt.* **1990**, *29*, 1526−1529.
(37) Maity, R.; Maiti, U. N.; Mitra, M. K.; Chattopadhyay, K. K. *Phys. E* **2006**, *33*, 104−109.
(38) Qi, L.; Mao, G. B.; Ao, J. P. *Appl. Surf. Sci.* **2008**, *254*, 5711−5714.